ORNL/TM-6564

Magnetic "Islandography" in Tokamaks

J. D. Callen
B. V. Waddell
H. R. Hicks
J. A. Holmes
D. K. Lee
S. J. Lynch
K. T. Tsang
J. C. Whitson
B. Carreras
M. Soler
M. Azumi
P. J. Catto
J. Smith

OAK RIDGE NATIONAL LABORATORY
OPERATED BY UNION CARBIDE CORPORATION · FOR THE DEPARTMENT OF ENERGY

BLANK PAGE

ORNL/TM-6564
Dist. Category UC-20 f and g

Contract No. W-7405-eng-26

FUSION ENERGY DIVISION

MAGNETIC "ISLANDOGRAPHY" IN TOKAMAKS*

J. D. Callen, B. V. Waddell, H. R. Hicks, J. A. Holmes,
D. K. Lee, S. J. Lynch, K. T. Tsang, J. C. Whitson

B. Carreras, M. Soler
Visitors from Junta de Energia Nuclear, Madrid, Spain

M. Azumi
Japan Atomic Energy Institute, Tokai, Japan

P. J. Catto
Science Applications, Inc., Boulder, Colorado

J. Smith
University of Tennessee, Knoxville, Tennessee

Date Published - September 1978

*Paper presented at the 7th International Conference on Plasma Physics & Controlled Nuclear Fusion Research, Innsbruck, Austria, August 23-30, 1978 (proceedings to be published).

Prepared by the
OAK RIDGE NATIONAL LABORATORY
Oak Ridge, Tennessee 37830
operated by
UNION CARBIDE CORPORATION
for the
DEPARTMENT OF ENERGY

CONTENTS

ABSTRACT

Tearing modes are shown to be responsible for most of the experimentally observed macroscopic behavior of tokamak discharges. The effects of these collective magnetic perturbations on magnetic topology and plasma transport in tokamaks are shown to provide plausible explanations for: internal disruptions (m/n = 1); Mirnov oscillations (m/n = 2,3,...); and major disruptions (coupling of 2/1-3/2 modes). The nonlinear evolution of the tearing modes is followed with fully three-dimensional computer codes. The effects on plasma confinement of the magnetic islands or stochastic field lines induced by the macroscopic tearing modes are discussed and compared with experiment. Finally, microscopic magnetic perturbations are shown to provide a natural model for the microscopic anomalous transport processes in tokamaks.

BLANK PAGE

1. INTRODUCTION

It is becoming increasingly clear that collective, helically resonant magnetic perturbations that produce field line breaking and thereby magnetic islands play a dominant role in the anomalous transport processes of internal disruptions, Mirnov oscillations, major disruptions, and anomalous electron heat conduction in present tokamak experiments. Even very small (e.g., $\tilde{B}_\theta/B \sim 10^{-4}$) magnetic perturbations can have significant effects on the magnetic topology and plasma transport because plasma transport is many orders of magnitude more rapid along magnetic field lines than across them. We first discuss generally in Section 2 the mechanisms by which magnetic perturbations arise, reconnect magnetic field lines to form magnetic islands, nonlinearly evolve, and ultimately affect plasma transport. Next, in Section 3 we discuss our nonlinear investigations of the macroscopic tearing instabilities made possible by development of single and multiple helicity resistive MHD computer codes. These macroscopic modes are considered from the lowest mode number upward, with emphasis on the nonlinear consequences of the modes and the increasingly detailed and favorable comparisons with tokamak experiments. In Section 4 we consider the (microscopic) high mode number finite β drift-Alfvén modes and their possible effect on transport in tokamaks. In Section 5 we summarize these investigations through the synthesis of a model of tokamak discharge behavior in terms of the effects of magnetic perturbations.

2. MAGNETIC ISLAND FORMATION AND EFFECTS IN TOKAMAKS

2.1 Magnetic Topology

Plasma equilibrium, stability, and confinement in a tokamak are provided by the rotational transform in the magnetic field induced by the toroidal current. In an axisymmetric tokamak the rotational transform produces toroidal magnetic flux surfaces whose cross sections are topologically nested circles. This simple magnetic topology can be destroyed by helically resonant, nonaxisymmetric magnetic perturbations. In the ideal MHD model, the Ohm's law $\underline{E} + \underline{V} \times \underline{B} = 0$ requires that the plasma move with the magnetic field; thus, it has been generally believed [1] that ideal MHD instabilities cannot change the topology of the flux surfaces. In real plasmas such as those confined in tokamaks, finite plasma resistivity and other irreversible kinetic effects admit collective magnetic perturbations that can "break" or reconnect magnetic field lines and thereby allow magnetic islands to form. The magnetic flux surfaces produced by a magnetic perturbation of given poloidal (m) and toroidal (n) mode number (i.e., a single helicity) can be simply computed in a long, straight, periodic cylinder model of a tokamak plasma. Namely, with the helical angle variable $\eta \equiv nz/R_0 - m\theta$ and all quantities constant in the helical (i.e., ignorable coordinate) direction $\underline{h} \equiv \underline{\eta} \times \hat{\mathbf{r}} = [\hat{z} + (nr/mR_0)\hat{\theta}]/\sigma$, the magnetic field can be written as

$$\underline{B} = B_h \underline{h} + \underline{h} \times \underline{\nabla}\psi_* \ , \tag{1}$$

where $\sigma = 1 + (nr/mR_0)^2$, with R_0 being the major radius. The $\underline{h} \times \underline{\nabla}\psi_*$ part is the "auxiliary" magnetic field $\underline{B}_*$ first introduced by Kadomtsev and Pogutse [2,3]. In terms of a cylindrical coordinate system the magnetic field components in the helical coordinate system are: $B_h = B_z + (nr/mR_0)B_\theta$, $B_r = (m/r)\partial\psi_*/\partial\eta$, $B_\eta = -\partial\psi_*/\partial r = -B_\theta + (nr/mR_0)B_z$. Here $\underline{B}$ comprises both the equilibrium and perturbation ($\tilde{\underline{B}}$) magnetic fields, with the dominant perturbation being in B_r since the equilibrium has no such component. Further, ψ_* is a

(helical) magnetic flux function in whose contours the magnetic field lines lie. As illustrated in Fig. 1, magnetic islands of width $w \sim \tilde{\psi}^{1/2} \sim \tilde{B}_r^{1/2}$ form in the vicinity of a rational surface (r_s) at which the flux function is extremal and hence most sensitive in the absence ($\eta = \pi/2$) of a magnetic perturbation.

2.2 Nonlinear Evolution

The nonlinear evolution of magnetic perturbations is complicated by the concomitant changes in magnetic topology and consequent modifications of plasma profiles. A single helicity magnetic perturbation produces a magnetic island of finite width. A number of things can happen as the magnetic perturbation grows due to a plasma instability. First, the (resistive) external flows induced by the growing island can cause the island growth to be reduced from exponential to only linear [4]. When only a single helicity mode is present the mode can saturate due to its quasilinear modification of the current profile [5], e.g., as in m = 2 tearing modes leading to Mirnov oscillations [6]. If two or more modes with incommensurate helicities are initially unstable, and when the amplitudes of the magnetic perturbations involved become large enough, there is another very important process that occurs—field lines stochastization. Roughly speaking, as shown in Fig. 2, if the magnetic islands produced by magnetic perturbations of different helicities overlap, then the magnetic field lines become stochastic [7] in the region encompassed by the two or more original magnetic islands, i.e., there are no well formed magnetic flux surfaces in this region. In the nonlinear evolution process the onset of significant field line stochastization has been found in the disruptive instability model [8] in Section 3 to be characterized by an explosive transfer of energy via mode coupling from the dominantly growing mode or modes into other modes of incommensurate helicity.

2.3 Effects on Plasma Transport

Since plasma transport is many orders of magnitude more rapid along magnetic field lines than perpendicular to them, we expect most plasma properties to be constant along magnetic field lines. Thus, for a single magnetic island or a discrete set of well separated magnetic islands, the plasma temperature and other plasma parameters should be nearly constant along helical flux contours such as those shown in Fig. 1. Microscopic plasma transport is not directly enhanced by the presence of a magnetic island; rather, because flux surfaces on opposite sides of an island nearly touch at the x points of the separatrix, the island just provides a transport "short circuit" over the physical region encompassed by the island. When magnetic islands of different helicity overlap to such an extent that the magnetic field lines become stochastic, plasma transport becomes considerably more complex. To the extent that a particular plasma property can be aware of the stochastization of the magnetic field lines (e.g., by propagation at the finite thermal speed), that plasma property will presumably be transported rapidly through the region of stochasticity. Since for roughly equal electron and ion temperatures the electron thermal speed is $\sqrt{m_i/m_e} \sim 40$ times greater than the ion thermal speed, the electron temperature profile is most quickly flattened when the field lines become stochastic. Runaway electrons, at least for low energies such that their radial drift orbit excursions are small, follow the magnetic field lines directly [9] whether they have a magnetic island or stochastic character.

3. TEARING MODES AND THEIR EFFECTS IN TOKAMAKS

3.1 Resistive MHD Models

A cylindrical model of the macroscopic tearing modes [10] in which the plasma pressure is ignored ($\beta \lesssim \varepsilon^2$ [11]) will be sufficient for our primarily nonlinear investigations. We begin from the resistive fluid equations and make the usual assumptions [2] that: 1) the coupling to compressional Alfvén modes, which keeps the radial component of the force balance in equilibrium (i.e., $\nabla p = \underline{J} \times \underline{B}$), can be neglected and hence the toroidal magnetic field B_z is unchanged by the tearing modes; and 2) the macroscopic flow velocity along the z direction is negligibly small. Then, the components of both the magnetic field and fluid flow velocities in the plane perpendicular to the z direction can be represented in terms of stream functions and the resistive fluid equations can be reduced in dimensionless form to [12,13]

$$\frac{\partial \Psi}{\partial t} + \underline{V}_\perp \cdot \underline{\nabla} \Psi = \eta_\parallel J_\zeta - \frac{\partial \Phi}{\partial \zeta}$$

$$\frac{\partial U}{\partial t} + \underline{V}_\perp \cdot \underline{\nabla} U = -S^2 \left[\hat{\zeta} \cdot (\underline{\nabla} \Psi \times \underline{\nabla} J_\zeta) + \frac{\partial J_\zeta}{\partial \zeta} \right] \tag{2}$$

with $J_\zeta = \nabla_\perp^2 \Psi$, $\underline{V}_\perp = \underline{\nabla} \Phi \times \hat{\zeta}$, and $U = \nabla_\perp^2 \Phi$. Here, $\zeta \equiv z/2\pi R_0$ is a normalized longitudinal cylindrical coordinate that represents the toroidal angle coordinate. The perpendicular magnetic field is given in terms of the poloidal flux function ψ by the relation $\underline{B}_\perp = \varepsilon B_z \underline{\nabla} \Psi \times \hat{\zeta}$, where $\varepsilon \equiv a/R_0$, with a being the minor radius of the torus. Since for our model B_z is independent of ζ, the helical flux function ψ_* defined in Eq. (1) is related to the poloidal flux function Ψ by $\psi_* = -(a^2 B_z/R_0)\Psi - (n/2mR_0)(r^2 - a^2)B_z$. The helical flux function ψ_* is most convenient for single helicity cases; is used for multiple helicity cases. In Eq. (2) the $\perp$ subscript means perpendicular to $\hat{\zeta}$, the unit vector along z; $V_\perp$, $\eta_\parallel$, J_ζ, Φ, and U are the velocity perpendicular to $\hat{\zeta}$, parallel plasma resistivity, toroidal current density, velocity stream function, and ζ component of the fluid vorticity, respectively. Equations (2) are in dimensionless form: the time is normalized to the resistive skin time, $\tau_R \equiv a^2 \mu_0/\eta_0$ where η_0 is the resistivity at $r = 0$. The quantity $S \equiv \tau_R/\tau_{Hp}$, where τ_{Hp} is the poloidal Alfvén time $R_0(\mu_0 \rho_0)^{1/2}/B_z$ in which ρ_0 is the (constant) mass density. The parameter S ranges from less than 10^4 for small ($a < 10$ cm), relatively cold ($T_e < 100$ eV) tokamak plasmas up to about 10^7 in PLT ($a \sim 40$ cm, $T_e \sim 1$ keV). The fact that this parameter is very large causes the greatest complication in the numerical solution of Eqs. (2) and necessitates the use of a very fine radial grid in the vicinity of a rational surface as well as an implicit time step scheme to make the problem tractable in a reasonable amount of computer time.

While analytic solutions of the linearized forms of Eqs. (2) can be derived in slab geometry [10], numerical solutions are required for studying the linear growth phase of modes extending over the entire cylindrical radius of the plasma and certainly for studying the nonlinear behavior. The computer codes currently being used at ORNL [5,12,14,15] to investigate tearing modes are listed in Table I. A recent computational accomplishment of major significance has been the development of the Fourier transform (or series) code RSF, in which the finite differencing in θ, ζ has been replaced by Fourier series representations in these periodic coordinates. RSF requires significantly fewer representation points

than the MASS code (finite difference) for the same degree of convergence and thus runs about 100 times faster. Consequently RSF is capable of treating much larger values of S than MASS in a reasonable amount of computer time. In addition to these linear and nonlinear codes for analyzing tearing modes, we have developed a code which follows magnetic field lines in the presence of the flux functions computed from Eqs. (2) and obtains results such as those illustrated in Fig. 2.

3.2 m/n = 1 (Internal Disruptions)

The m = 1 tearing mode is the dynamic mechanism which causes the abrupt drop phase in internal disruptions or sawtooth oscillations [16]. The mode begins to grow whenever q drops below unity at the plasma center, thereby inducing shear at the q = 1 surface r_s. Single helicity numerical calculations [14] have shown that the mode continues to grow until the magnetic topology flips [3,17]; the magnetic island it produces becomes so large that the magnetic axis of the island moves toward the geometric center of the plasma and thereby transforms the magnetic topology of the central core from the original one centered about the central magnetic axis to one centered about the magnetic island center (which, however, is at that point near the geometric center of the plasma). While the 2/2 and 3/3 modes are usually linearly unstable as well and the mode coupling effects prevent stabilization at a narrow island width, the basic nonlinear stabilization mechanism is a quasilinear one—because the mode becomes stable after reconnection into the final state.

Since the m = 1 tearing mode growth rate is much faster than the ohmic heating rate, the electron temperature is equilibrated along all of the reconnecting magnetic field lines and hence is flattened within the induced m/n = 1 magnetic island. Ultimately, the region over which the electron temperature flattens extends, from flux conservation considerations [3], out to $r_0 \sim \sqrt{2} r_s$. Thus, immediately after the internal disruption, the temperature profile is flat within the radius r_0. Thereafter, on a much slower time scale, the combination of ohmic heating and radial electron heat transport reheats the plasma center back toward the centrally peaked electron temperature and current density profiles. An analytic model of internal disruptions [18,19], which is based on the cyclic process [20,21] in which the plasma core resistively overheats and drives q below unity, causing the m = 1 tearing mode to become unstable with an accelerating growth rate and ultimately to flatten the electron temperature profile as magnetic reconnection occurs, has been developed. It has been extensively and quite favorably compared with ORMAK data on the space-time evolution of internal disruptions and their m = 1 precursors [18,19].

Because internal disruptions abruptly change the electron temperature profile to a nonequilibrium state, they provide a valuable tool for experimentally examining the electron heat transport process. By following the space-time evolution of the electron temperature profile outside r_0, it has been shown [19,22] from ORMAK data that the anomalous electron heat transport process governing heat transport between internal disruptions is a diffusive process on scale lengths less than about 2 cm and that [19,22] the electron heat conduction coefficient governing this diffusive process is, to within experimental error, the same as that governing electron heat transport in the background plasma. Similar results and conclusions have been obtained from Alcator data [23]. Thus, internal disruptions affect plasma transport only through the changes in magnetic topology and whatever causes the anomalous electron heat transport in tokamaks must be microscopic (i.e., <1-2 cm in scale length) in origin.

3.3 m/n = 2 (Mirnov Oscillations)

An elementary quasilinear tearing mode theory in cylindrical geometry [5] accurately gives the amplitude of the m = 2 poloidal magnetic field fluctuations (Mirnov oscillations [25]) at the tokamak limiter [6]. The input required is the electron temperature radial profile, from which the current density and corresponding safety factor profile can be inferred. The saturation amplitude is obtained from a semianalytic nonlinear Δ' analysis that uses DELSOL. The mode is assumed to saturate when the discontinuity in the radial derivative of the flux function, as measured in the presence of the associated magnetic island, vanishes:

$$\Delta'(w) \equiv [(d\psi_{21}/dr)_{r_+} - (d\psi_{21}/dr)_{r_-}]/\psi_{21}(r_s) = 0 \qquad (3)$$

where $r_\pm = r_s \pm w/2$, in which w is the magnetic island width. In the linear theory δW energy is proportional [11] to the linear Δ'; thus, this assumption appears equivalent to assuming that the mode saturates when the nonlinear δW vanishes. Fully nonlinear simulations with the MASS and RSF codes are used to confirm the saturated island widths obtained from Eq. (3) with DELSOL and to verify that the saturation mechanism is a quasilinear one; for experimentally relevant q profiles, the results usually agree within 20%.

Typical results obtained from this procedure are shown in Fig. 3. The maximum saturated island widths for these m = 2 tearing modes occur when the singular surface approaches but stays somewhat inside the wall at r = a. Since in determining the saturated island width we calculate the full radial structure of the tearing mode, as shown in Fig. 3b one can also compute the magnetic field that would be seen on a probe near the limiter. A direct comparison [6] of this theory with the Mirnov oscillations observed in ORMAK [24] is shown in Fig. 4. The electron temperature profiles used in these calculations are experimentally measured and are different for different q(a). Similarly favorable comparisons have also been made with data from T-4 [6]. We believe that this excellent qualitative and quantitative correlation between the nonlinear tearing mode theory and experimental data conclusively proves that Mirnov oscillations are simply nonlinearly saturated tearing modes of a single helicity—m/n = 2 here, but more generally any single mode with $m/n \neq 1$.

An understanding of Mirnov oscillations is important because [26] their amplitude correlates with the overall plasma confinement time τ_E as shown in Fig. 4. In order to determine if simple ergodic effects are responsible for the variation in τ_E, the magnetic field structure produced by the interaction of the 2/1 tearing mode with the 1/R falloff of the equilibrium magnetic fields has been studied numerically and analytically [7]. Although the field lines are found to be ergodic near the separatrix, the region of ergodicity is too small to appreciably affect the transport. In order to calculate the effect of the presence of the induced magnetic island on τ_E, we have derived [27] plasma transport equations in the helical flux coordinates given in Eq. (1). To lowest order, the very rapid transport along field lines causes the plasma parameters to be only a function of ψ_*. To next order, there are small plasma parameter variations within a given helical flux surface (cf. Fig. 1) due to the $\underline{B} \times \underline{\nabla}(p,T)$ contributions to the mass and heat flux. The latter effect leads to (negligible) Pfirsch-Schlüter-type contributions to transport fluxes. The dominant effect of the magnetic island is to change the metric elements in the

perpendicular heat diffusion operator in the vicinity of the island due to the change in topology. The boundary conditions imposed are temperature continuity and a jump condition in the heat flux from one side of the island to the other, given by the amount of heat diffusing out from the center of the island. Roughly speaking, the dominant effect on transport is to remove from the confinement region that area occupied by the magnetic island and thereby to reduce proportionally the energy containment time in the plasma. For the idealized model of heat sources and electron heat conduction that are spatially constant, the plasma energy containment time is decreased by a factor of $[1 - (w/a)(4r_s^3/a^3)]$. For spatially varying heat sources and conduction coefficients, the multiplier of w/a can change by a factor of two or more. From Figs. 3 and 4 we see that since both r_s/a and w/a increase significantly as q(a) decreases below 6, the falloff of τ_E with decreasing q(a) could be due to the transport short circuit effect of the Mirnov oscillation-induced magnetic island. On the other hand, for $q(a) > 6$ in ORMAK the islands shrink and move toward the center of the plasma, where their effect on τ_E becomes negligible. Thus, in the universal scaling curves of τ_E versus q(a) postulated by Mirnov [26], the falloff at low q(a) might be explained by the correlated $\tilde{B}_\theta$ (Mirnov) oscillations, but the gentle increase of τ_E with decreasing q(a) at high q(a) is apparently not due to the effects of Mirnov oscillations.

For hollow electron temperature profiles such as can be produced during the current initiation phase of tokamak discharges, or when there is too much impurity radiation from the plasma center, two singular surfaces of the same helicity (e.g., 3/1) can occur within the plasma. Then, if tearing modes are unstable at both these surfaces, two sets of magnetic islands develop during the nonlinear evolution phase. The final state is found [28] to be characterized by one of two possibilities: saturation—the two modes saturate quasilinearly separately or while intertwining in much the same manner as Mirnov oscillations; reconnection [3]—the two islands interact and the field lines reconnect into a new axisymmetric equilibrium for which the q profile is flat with $q \approx m/n$. We find numerically that the reconnection process occurs whenever $\psi_*(0) \approx \max \psi_*(r > 0)$. The reconnection case is very similar to the evolution of $m/n = 1$ modes into internal disruptions and is probably the mechanism behind the increased MHD activity occuring during current initiation [29] and with hollow electron temperature profiles, e.g., the $m = 3$ disruption in PLT [30]. The electron temperature profile should become flattened over the reconnection region, but because of the fact that good, if a bit contorted, flux surfaces exist throughout the reconnection process, one would expect a redistribution with no direct loss of the energy stored in the plasma.

3.4 Interaction of 2/1 and 3/2 Modes (Major Disruptions)

For q(r) profiles observed prior to major disruptions, the 3/2 tearing mode as well as the 2/1 mode is often strongly unstable in linear theory; then the single helicity model used to obtain Figs. 3 and 4 is not valid. Consequently, we have investigated the hypothesis [8] that the major disruption in tokamaks is due to the interaction of tearing modes of incommensurate helicity. The essential results [8,12,31] from the two codes RS3 and RSF, as illustrated in Fig. 5a, are that on a rapid time scale the 2/1 mode destabilizes the other modes, particularly the 3/2 mode and those with helicities between 3/2 and 2/1. The corresponding deformations of the current density profile in the initial (t_1), predisruption (t_2), and disruption (t_3) states indicated in Fig. 5a are shown in Fig. 5b. The magnetic field topologies corresponding to the times t_2 and t_3 in

Fig. 5 are those shown in Figs. 2a and 2b, respectively. Clearly, the ultimate effect of the nonlinear 2/1-3/2 coupling is a severe deformation of the current profile and the destruction of the magnetic flux surfaces over a sizeable portion of the plasma. If the radius of the 2/1 singular surface is large enough initially, the disrupted region can extend to the plasma limiter. The computer runs [12] are terminated shortly after destruction of the magnetic flux surfaces because of limitations in the present model: 1) the extreme nonlinearity, which cannot be adequately modeled by the finite number (typically 22 or 40) of modes being considered; and 2) the lack of a simultaneous calculation of the electron temperature profile, which would surely be flattened over the stochastic region at time t_3 and lead to a corresponding flattening of the current profile. As a rough criterion, field line stochastization and hence a disruptive instability occur when two or more islands of incommensurate helicity are estimated initially to overlap, i.e., $(w_{21} + w_{32})/2 > r_{21} - r_{32}$, where the island widths of the 2/1 and 3/2 modes are determined from Eq. (3).

To develop a model for the dynamics of a disruptive instability we examine [31] the mechanisms responsible for the explosive growth of all but the basic 2/1 mode after time t_2 in Fig. 5a. First, we note that before t_2 the 2/1 and 3/2 islands are growing roughly linearly with time, in agreement with previous theory [4] for this high S regime. After time t_2, the quasilinear effect of the 2/1 mode on the q profile is found [12,31] to destabilize the 3/2 and 5/3 modes, but not nearly as greatly or rapidly as is observed in Fig. 5a. Thus an analytic mode coupling model [31] has been developed for the nonlinear interaction in the low S regime where the tearing width exceeds the island width. The phenomenological model shows that the decrease in the growth rate of the 2/1 mode after time t_2 in Fig. 5a is due to the modification of the equilibrium by the 2/1 mode itself. The 1/1 and 5/3 modes are essentially driven by the 2/1 and 3/2 modes. Then, in turn, the 5/3 and 1/1 modes couple with the 2/1 mode to further destabilize the 3/2 mode. Scaling laws developed [31] for the maximum growth rate and time of its occurrence for the various modes in Fig. 5a were found to agree with computer runs for $3 \times 10^4 < S \lesssim 10^6$, i.e., into the high S regime [4] as well. Apparently, the usual resistive flow effects that reduce the mode growth from exponential to linear [4] are not operative in this explosive growth phase because the magnetic flux surfaces are being destroyed. Since the explosive growth of the 3/2 mode is what causes the onset of stochasticity in the magnetic field lines, we propose that the time scale for a major disruption Γ is this growth time, which is found from the model [31] to be roughly the linear growth time of the 2/1 tearing mode, γ_{21}^{-1}.

Three key features of this model of major disruptions correlate well with tokamak experimental results. First, the disruptions observed in Alcator, LT-3, PLT, and T-4 are asymmetrical in the poloidal plane, which means that modes odd in m, such as the 3/2 and 1/1 modes, are excited during the disruption process. Second, since the current density profile broadens significantly during the disruption, the internal inductance decreases and, as observed experimentally, there should be a large negative voltage spike. Thirdly and more quantitatively, as shown in Fig. 6, the experimentally observed time scale for major disruptions does correlate reasonably well with the theoretical estimate $\Gamma \sim \gamma_{21}^{-1} \sim \tau_R^{3/5} \tau_{Hp}^{2/5}$.

Because major disruptions can have disastrous effects on the plasma, one would like to avoid them. From the model presented above, we see that the key element in avoiding them is to prevent the 2/1-3/2 island overlap interaction. Since the 2/1 mode is centered at a larger and hence more accessible radius and since it sometimes has a slower growth phase, the most direct way to control

disruptions is by feedback control of the 2/1 mode amplitude in such a way that the 3/2 mode is not destabilized. This can be accomplished either by a direct feedback stabilization of the mode or by localized heating to modify the current profile (cf. Fig. 3a). The feasibility of both methods has been confirmed with detailed computations. In the feedback calculations it is critical to have both a very short (compared to γ_{21}^{-1}) time delay and response time of the feedback system, in order to prevent the growth of the regular 2/1 mode or its near mirror image, for which the sign of the 2/1 Fourier mode is reversed over most of the plasma.

4. MICROINSTABILITIES AND THEIR EFFECTS

As shown explicitly by the analysis of electron temperature perturbations induced by internal disruptions, the macroscopic tearing modes discussed in the preceding section do not seem to have any direct effect on the microscopic transport processes. Most calculations of anomalous transport are based on electrostatic drift wave turbulence. In parallel with the preceding discussion of the magnetic perturbation effects arising from macroscopic tearing modes, we discuss the alternative (and we believe more probable) hypothesis [32] that the typically small magnetic component of microinstabilities due to finite β is the dominant mechanism which, through magnetic topology effects, causes anomalous transport in tokamaks.

4.1 Finite β Microinstabilities in Tokamaks

Both electrostatic drift waves and shear-Alfvén modes can be unstable in a collisionless plasma in the local approximation. However, in a tokamak the sheared magnetic field invalidates the local approximation and one must solve a radial eigenmode problem in order to determine the stability of the modes. Very accurate computer codes have been developed [33] at ORNL to solve the relevant equations [34]. Using these codes it has been shown that, in contrast to previous work [35], electrostatic collisionless drift modes are stable for all reasonable magnetic shear levels [36]. It has recently been shown [37] that finite β effects generally have a further stabilizing influence on these drift modes. In addition, we have found [37] a collisionless shear-Alfvén mode; this mode is also damped, but with a damping decrement that generally decreases as β increases. Nonetheless, at least for present models [34], whose validity is being reexamined in more detail, both modes can become unstable when trapped electron effects are added [37]. The magnetic component of both the drift- and shear-Alfvén microinstabilities provides a natural vehicle for microscopic magnetic turbulence in tokamaks.

4.2 Anomalous Transport Due to Magnetic Microturbulence

At very low amplitudes microscopic magnetic perturbations produce nonoverlapping magnetic islands in the same way that the macroscopic modes do [cf. Eq. (1) and Figs. 1,2a]. At this low level, if there is some extrinsic mechanism that determines the growth and decay rate γ for the microinstabilities, the electron heat conduction coefficient induced by the birth and death of microscopic magnetic islands is estimated "quasilinearly" to be [32] $\chi_e^w \sim (3/16)(\gamma + \nu)w^2$, where ν is the collision frequency. By analogy with the nonlinear evolution of the macroscopic modes discussed above, we expect the most significant transport to occur when two islands begin to overlap and thereby destroy the magnetic flux surfaces locally. While the induced transport has not been calculated in detail for this case, it is presumably similar in form to the

quasilinear result [32] with the island width replaced by the initial island separation. If the drift wave-induced magnetic perturbations can continue to grow in the presence of stochastic field lines, they could produce totally ergodic field lines over the entire plasma cross section. Then the radial electron heat transport can be computed by a statistical process [38]. With irregular field line and/or island topologies, electrons try to diffuse radially more rapidly than the ions; however, a radial potential builds up [32] to confine electrostatically all but runaway electrons and thereby keep the particle diffusion ambipolar. Thus, the generic consequences [32] of "magnetic flutter" models of anomalous transport are that: 1) the runaway electron containment time should be comparable to the overall electron energy containment time; 2) electron temperature fluctuations should be larger than density fluctuations; and 3) radial electron heat conduction should be the dominant nonradiative loss process. All three of these generic consequences are observed in tokamak experiments. Thus, while there does not yet exist a complete theory that correctly predicts the scaling and magnitude of the anomalous electron heat conduction coefficient, the magnetic flutter models are an encouraging avenue to follow to resolve this major enigma of transport in tokamaks.

5. SUMMARY—PLASMA DISCHARGE MODEL FOR TOKAMAKS

As we have shown, most of the experimentally observable macroscopic behavior of tokamak discharges can be correlated with the nonlinear effects of low mode number tearing modes on magnetic topology and plasma transport. Based on our model we see that during the current initiation phase, skin currents are relaxed by the nonlinear evolution of the islands induced by a double tearing mode which, given the right conditions, flattens the current profile all the way to the plasma center [28,29] but does not destroy confinement. Thereafter as the plasma comes into quasi-equilibrium at the desired current level, many things can happen. If, through the evolution of transport processes determining the q profile, q at the center drops below unity, m/n = 1 tearing modes grow at the q = 1 surface and cause an internal disruption [16] that flattens the electron temperature profile out to a radius $r_0 \sim \sqrt{2} r_s$. As long as r_0 is small compared to the limiter radius, internal disruptions do not have any externally observable effect on the plasma energy confinement time τ_E. Often the q profile is such that an m/n = 2/1 tearing mode is unstable and it grows to a saturated state where it is observed experimentally as a Mirnov oscillation [25]. The induced magnetic islands are typically small (cf. Figs. 3,4) and although they provide a transport short circuit over the region they inhabit (cf. Fig. 1), their effect on τ_E is small (cf. Fig. 4) except at low q(a), where their width and radial location are large. Then, they can lead to a deterioration of τ_E by up to a factor of two, in agreement with the low q(a) portion of the Mirnov universal scaling curve for τ_E [26]. For discharges which obtain a hollow temperature profile, presumably through excessive radiation from impurities at the center, a double tearing mode can occur and cause the central q and temperature profiles to flatten in much the same way as occurs in the internal disruption. Finally, the disruptive instability can occur if by virtue of internal disruptions of a single or double tearing mode type and/or transport processes, the q profile admits tearing modes of incommensurate helicity (in particular, 2/1 and 3/2) that are strongly unstable in linear theory. The linearly unstable modes of different helicity are found to grow to an explosive mode coupling stage (cf. Fig. 5) where the magnetic flux surfaces are destroyed over a significant region of the plasma (cf. Fig. 2). This stochastic magnetic field region can encompass the plasma limiter and undoubtedly leads to a drastic reduction in plasma confinement.

When the effects of all these macroscopic phenomena have been minimized, there still remains anomalous transport, which apparently must be microscopic in origin. The magnetic perturbation effects of finite β drift- and shear-Alfvén waves with trapped particle effects included provide a natural vehicle for "magnetic flutter" models of anomalous transport. The latter models, although encouraging in their generic correlation with experimental results, have not yet yielded an explanation for the anomalous transport.

ACKNOWLEDGMENT

The authors gratefully acknowledge useful discussions with J. T. Hogan, W. A. Houlberg, O. P. Manley, M. Murakami, and N. Sauthoff. They are also grateful to S. V. Mirnov and Yu. N. Dnestrovskii for providing early copies of Refs. [26] and [29].

REFERENCES

[1] Some counter-examples to this statement have been proposed by GRAD, H., "Reconnection of Magnetic Field Lines in an Ideal Fluid," NYU Courant Institute Report, MF-92, April 1978.
[2] KADOMTSEV, B. B. and POGUTSE, O. P., Sov. Phys.-JETP 38 (1974) 283.
[3] KADOMTSEV, B. B., Sov. J. Plasma Phys. 1 (1976) 389.
[4] RUTHERFORD, P. H., Phys. Fluids 16 (1973) 1903.
[5] WHITE, R. B., MONTICELLO, D. A., ROSENBLUTH, M. N., and WADDELL, B. V., Phys. Fluids 20 (1977) 800.
[6] CARRERAS, B., WADDELL, B. V., and HICKS, H. R., "Poloidal Magnetic Field Fluctuations in Tokamaks," ORNL/TM-6403, July 1978.
[7] RECHESTER, A. B. and STIX, T. H., Phys. Rev. Lett. 36 (1976) 587.
[8] WADDELL, B. V., CARRERAS, B., HICKS, H. R., HOLMES, J. A., and LEE, D. K., "A Mechanism for Major Disruptions in Tokamaks," ORNL/TM-6213, June 1978.
[9] ZWEBEN, S. J., WADDELL, B. V., SWAIN, D. W., and FLEISCHMAN, H. H., "High Energy Runaway Orbits in the Presence of m = 2 Magnetic Islands," ORNL/TM-6216, July 1978.
[10] FURTH, H. P., KILLEEN, J., and ROSENBLUTH, M. N., Phys. Fluids 6 (1963) 459; FURTH, H. P., RUTHERFORD, P. H., and SELBERG, H., Phys. Fluids 16 (1973) 1054.
[11] GLASSER, A. H., GREENE, J. M., and JOHNSON, J. L., Phys. Fluids 18, (1975) 875.
[12] HICKS, H. R., CARRERAS, B., HOLMES, J. A., and WADDELL, B. V., "Interaction of Tearing Modes of Different Pitch in Cylindrical Geometry," ORNL/TM-6096, December 1977.
[13] STRAUSS, H. R., Phys. Fluids 19 (1976) 134; BISKAMP, D., private communication (1977).
[14] WADDELL, B. V., ROSENBLUTH, M. N., MONTICELLO, D. A., and WHITE, R. B., Nucl. Fusion 16 (1976) 528.
[15] HICKS, H. R., CARRERAS, B., HOLMES, J. A., LEE, D. K., LYNCH, S. J., and WADDELL, B. V., "Fourier Transform vs. Finite Difference Techniques in Nonlinear Resistive MHD Codes," Computational Plasma Physics Meeting, Monterey, CA, June 1978, CONF-780614.
[16] VON GOELER, S., STODIEK, W., and SAUTHOFF, N., Phys. Rev. Lett. 33 (1974) 1201.
[17] TAYLOR, J. B., in Plasma Physics and Controlled Nuclear Fusion Research, 1974 (IAEA, Vienna, 1975), Vol. I, p. 161.
[18] WADDELL, B. V., JAHNS, G. L., CALLEN, J. D., and HICKS, H. R., Nucl. Fusion 18 (1978) 735; ORNL/TM-5840, May 1977.

[19] JAHNS, G. L., SOLER, M., WADDELL, B. V., CALLEN, J. D., and HICKS, H. R., Nucl. Fusion 18 (1978) 609.
[20] SYKES, A. and WESSON, J. A., Phys. Rev. Lett. 37 (1976) 140.
[21] DNESTROVSKII, Yu. N., LYSENKO, S. E., and SMITH, R., Sov. J. Plasma Phys. 3 (1977) 9.
[22] CALLEN, J. D. and JAHNS, G. L., Phys. Rev. Lett. 38 (1977) 491; SOLER, M. and CALLEN, J. D., "On Measuring the Electron Heat Diffusion Coefficient in a Tokamak from Sawtooth Oscillations," ORNL/TM-6165, February 1978.
[23] SOLER, M., CALLEN, J. D., NAVARRO, A. P., GRANETZ, R., SEGUIN, F., and PETRASSO, R., "Analysis of Heat Transport in Alcator from Sawtooth Observations" (to be published).
[24] BERRY, L. A. et al., in Plasma Physics and Controlled Nuclear Fusion Research, 1976 (IAEA, Vienna, 1977), Vol. I, p. 49.
[25] MIRNOV, S. V. and SEMENOV, I. B., Sov. J. of At. Energy 30 (1971) 22.
[26] MIRNOV, S. V., "On the Scaling Laws for the Energy Confinement Time in Tokamaks," Paper F-1-2, this conference.
[27] CALLEN, J. D. and AZUMI, M., "Plasma Transport in the Presence of a Magnetic Island" (to be published).
[28] CARRERAS, B., HICKS, H. R., and WADDELL, B. V., "Tearing Mode Activity for Hollow Current Profiles" (to be published).
[29] DNESTROVSKII, Yu. N., KOSTOMAROV, D. P., LYSENKO, D. E., PEREVERZEV, G. V., and TARASYAN, K. N., "Simulation of Discharge Dynamics in Tokamaks," Paper F-1-3, this conference.
[30] SAUTHOFF, N. R., VON GOELER, S., and STODIEK, W., "A Study of Disruptive Instabilities in the PLT Tokamak Using X-ray Techniques," PPPL-1379, January 1978.
[31] CARRERAS, B., WADDELL, B. V., and HICKS, H. R., "Analytic Model for the Nonlinear Interaction of Tearing Modes of Different Pitch in Cylindrical Geometry," ORNL/TM-6175, March 1978.
[32] CALLEN, J. D., Phys. Rev. Lett. 39 (1977) 1540.
[33] SMITH, J. and WHITSON, J. C., "A Numerical Study of the System of Differential Equations for the Drift Wave in Tokamaks," ORNL/CSD/TM-50, March 1978.
[34] CATTO, P. J., EL NADI, A. M., LIU, C. S., and ROSENBLUTH, M. N., Nucl. Fusion 14 (1974) 405; TANG, W. M., LIU, C. S., ROSENBLUTH, M. N., CATTO, P. J., and CALLEN, J. D., Nucl. Fusion 16 (1976) 191.
[35] PEARLSTEIN, L. D. and BERK, H. L., Phys. Rev. Lett. 23 (1969) 220.
[36] TSANG, K. T., CATTO, P. J., WHITSON, J. C., and SMITH, J., Phys. Rev. Lett. 40 (1978) 327; see also ROSS, D. W. and MAHAJAN, S. M., ibid., 324.
[37] TSANG, K. T., WHITSON, J. C., CALLEN, J. D., CATTO, P. J., and SMITH, J., "Drift Alfvén Waves in Tokamaks" (to be published in Phys. Rev. Lett.).
[38] RECHESTER, A. B. and ROSENBLUTH, M. N., Phys. Rev. Lett. 40 (1978) 38.

Table I. Tearing Mode Computer Codes Currently in Use at ORNL

NAME	CHARACTERISTICS	GEOMETRY/DIMENSIONS (HELICITIES)	NUMERICAL TECHNIQUE	CALCULATES	COMMENTS
LINEAL	Linear initial value code	Cylindrical/1 (single)	Finite difference in r	$\psi_{mn}(r,t)$	Used in profile explorations
DELSOL [5]	Linear boundary condition code	Cylindrical/1 (single)	Finite difference in r	Δ' and w_{mn}	Incorporated into Oak Ridge transport code
MASS [14]	Nonlinear initial value code	Cylindrical/2 (single)	Finite difference in r, η	ψ_s, Φ, T	Efficiency low compared with RSF, which effectively supercedes both these codes
RS3 [12]	Nonlinear initial value code	Cylindrical/3 (multiple)	Finite difference in r, θ, ζ	Ψ, Φ	
RSF [15]	Nonlinear initial value code	Cylindrical/3 (multiple)	Finite difference in r, Fourier transform in θ, ζ	Ψ, Φ, T, (n)	Feedback stabilization incorporated. (Diamagnetic effects being included.)
RS3T	Nonlinear initial value code	Toroidal/3 (multiple)	Finite difference in r, θ, ζ	Ψ, Φ	Under development

FIGURE CAPTIONS

Fig. 1. Helical flux function (a) and flux surfaces (b) at a z = constant plane in the presence of an m/n = 2/1 helical perturbation in the periodic cylinder approximation. For this particular case (B-2 of Ref. [6], q(a) = 4.0 in Fig. 4), the singular radius $r_s = 0.68a$ and the island width $w_{21} = 0.17a$.

Fig. 2. Illustration of the change in the magnetic field topology as the stochasticity parameter [7] s(≡ island width divided by distance between singular surfaces) increases from 0.88 (a) to 1.15 (b). In the initial case (a) there are prominent m/n = 2/1 and 3/2 magnetic islands and some very small 5/3 islands. In the final (stochastic) case (b) the motion of a single magnetic field line is shown to encompass ergodically a region that is only slightly greater than the region encompassed by the islands projected from the various helical harmonic components of the flux function, indicated by the weak dashed lines.

Fig. 3. Nonlinear saturation levels of (a) the island width w, and (b) the magnetic fluctuation level on an external probe ($\tilde{B}_\theta/B_\theta$) for m/n = 2/1 tearing modes as a function of the safety factor at the limiter q(a). Results are shown for three experimentally relevant models of the current profile specified through $q(r) = q(0)\left|1 + (r/r_0)^{2\lambda}\right|^{1/\lambda}$. As q(a) changes, r_0 is varied to keep q(0) = 1.

Fig. 4. Comparison of the theoretically predicted and experimentally measured external magnetic perturbations due to Mirnov oscillations for a sequence of ORMAK discharges with different q(a). Also shown is the variation of the energy containment time τ_E for this sequence [24].

Fig. 5. Growth of magnetic island widths (a) and corresponding deformation of the current density profile (b) for a case where initially both the 2/1 and 3/2 tearing modes are unstable. For this case modeling a PLT disruption [30], $S = 10^6$ and $q(r) = q(0)\left|1 + (r/r_0)^{2\lambda}\right|^{1/\lambda}$ with q(0) = 1.34, $r_0 = 0.56$, and $\lambda = 3.24$, which corresponds to the measured electron temperature profile.

Fig. 6. Comparison of the theoretical estimate $\Gamma \sim \gamma_{21}^{-1}$ with the experimentally observed disruption time Γ_D for various tokamaks [31]. The proportionality constant in the theory is normalized to yield exact agreement with the PLT point.

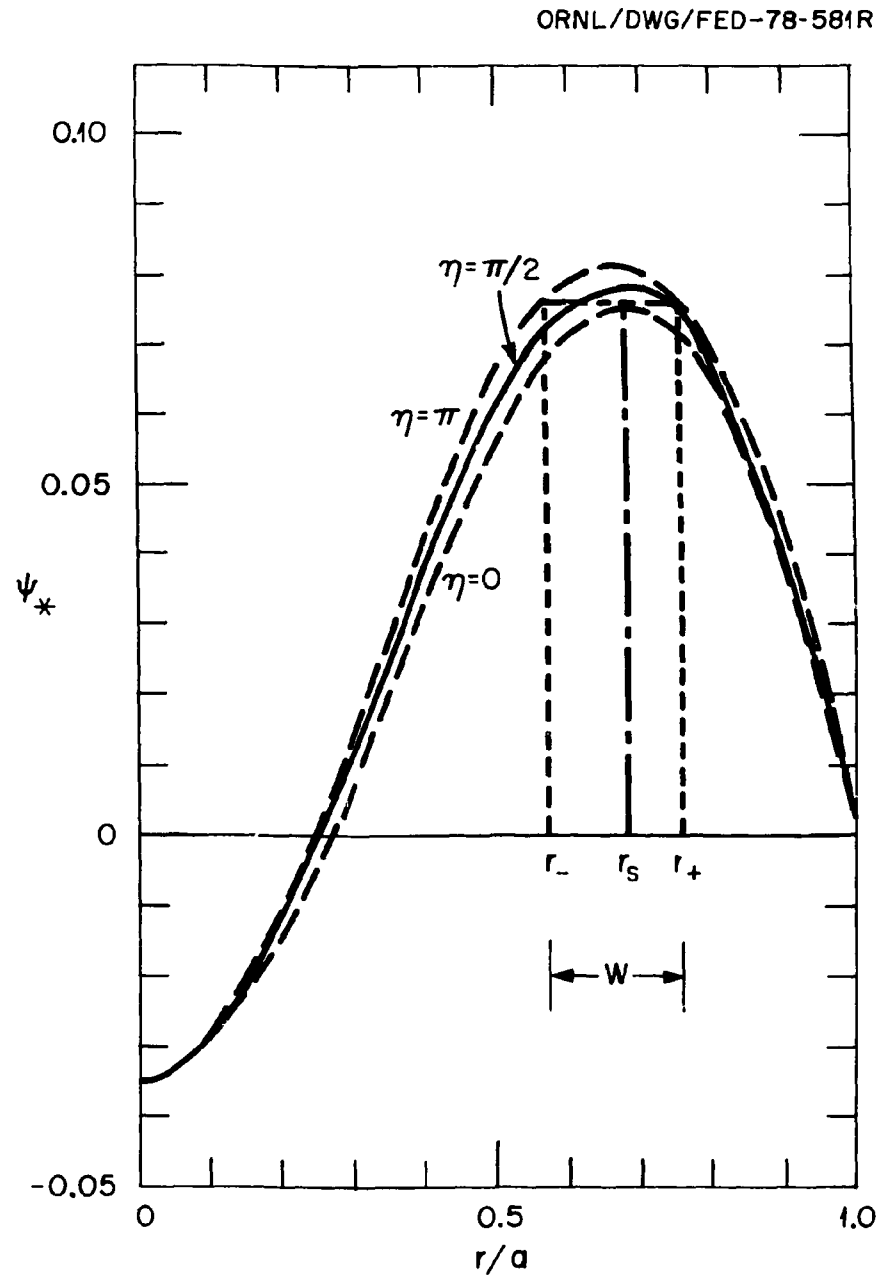
ORNL/DWG/FED-78-581R
0.10
0.05
0
-0.05
ψ_*
$\eta=\pi/2$
$\eta=\pi$
$\eta=0$
r_-
r_s
r_+
W
0
0.5
1.0
r/a

Fig. 1(a).

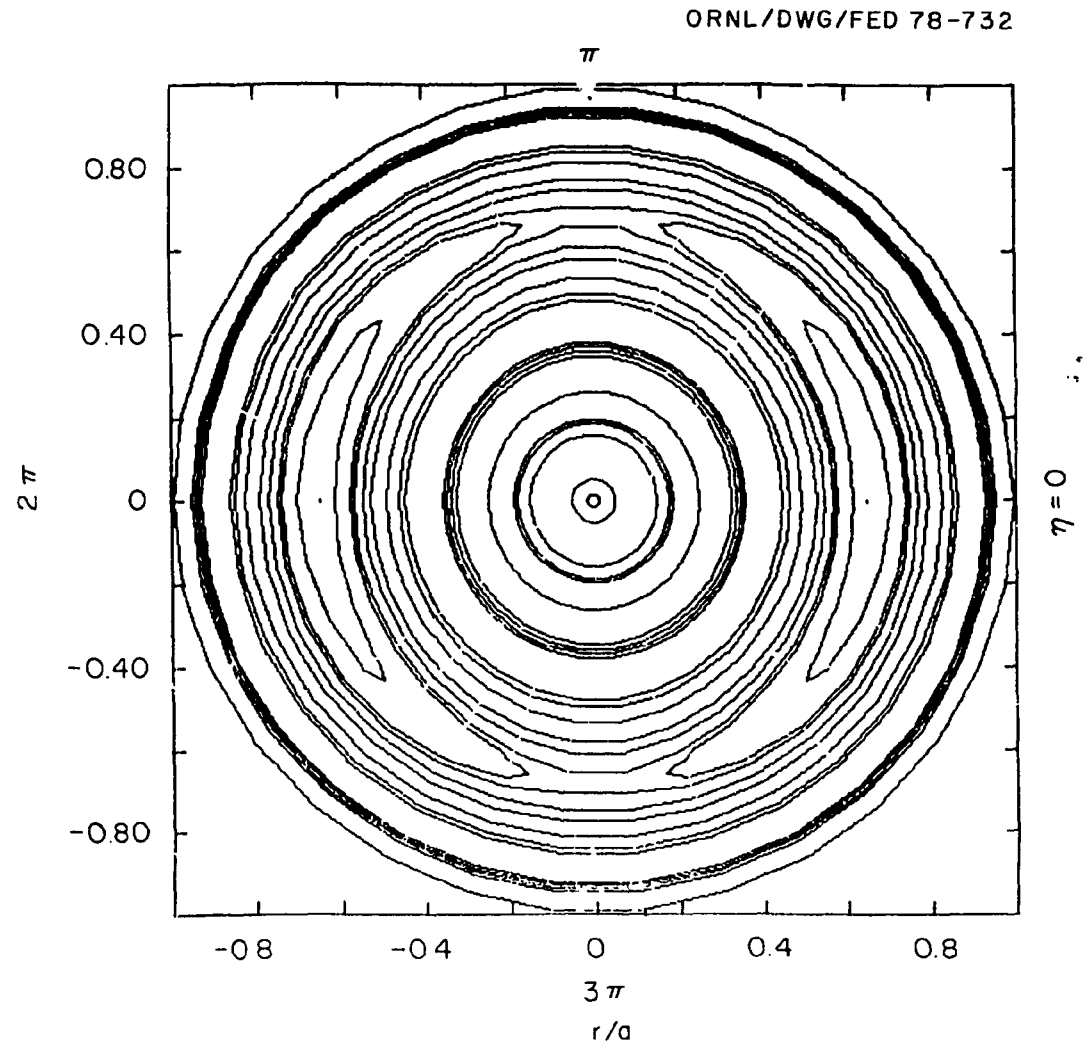

Fig. 1(b).

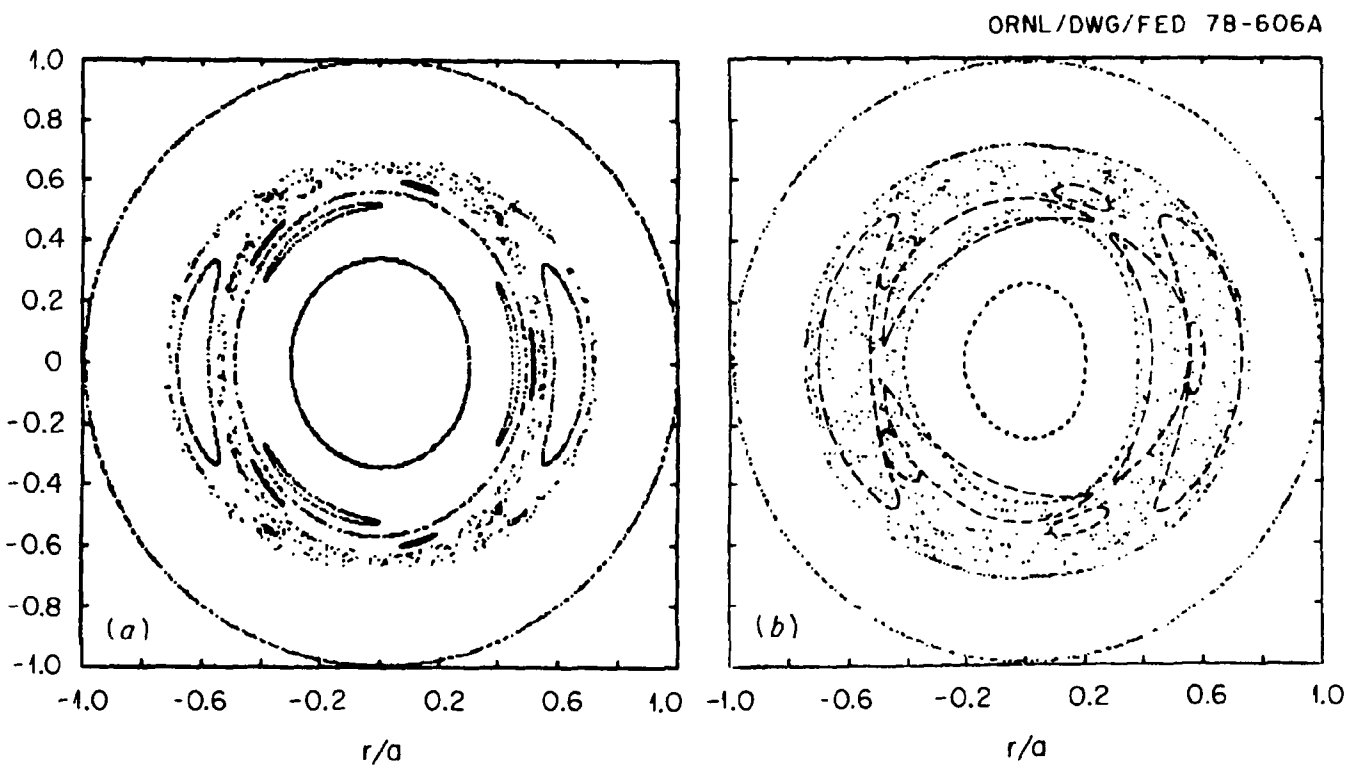
ORNL/DWG/FED 78-606A
1.0
0.8
0.6
0.4
0.2
0
-0.2
-0.4
-0.6
-0.8
-1.0
(a)
(b)
-1.0
-0.6
-0.2
0.2
0.6
1.0
r/a

Fig. 2.

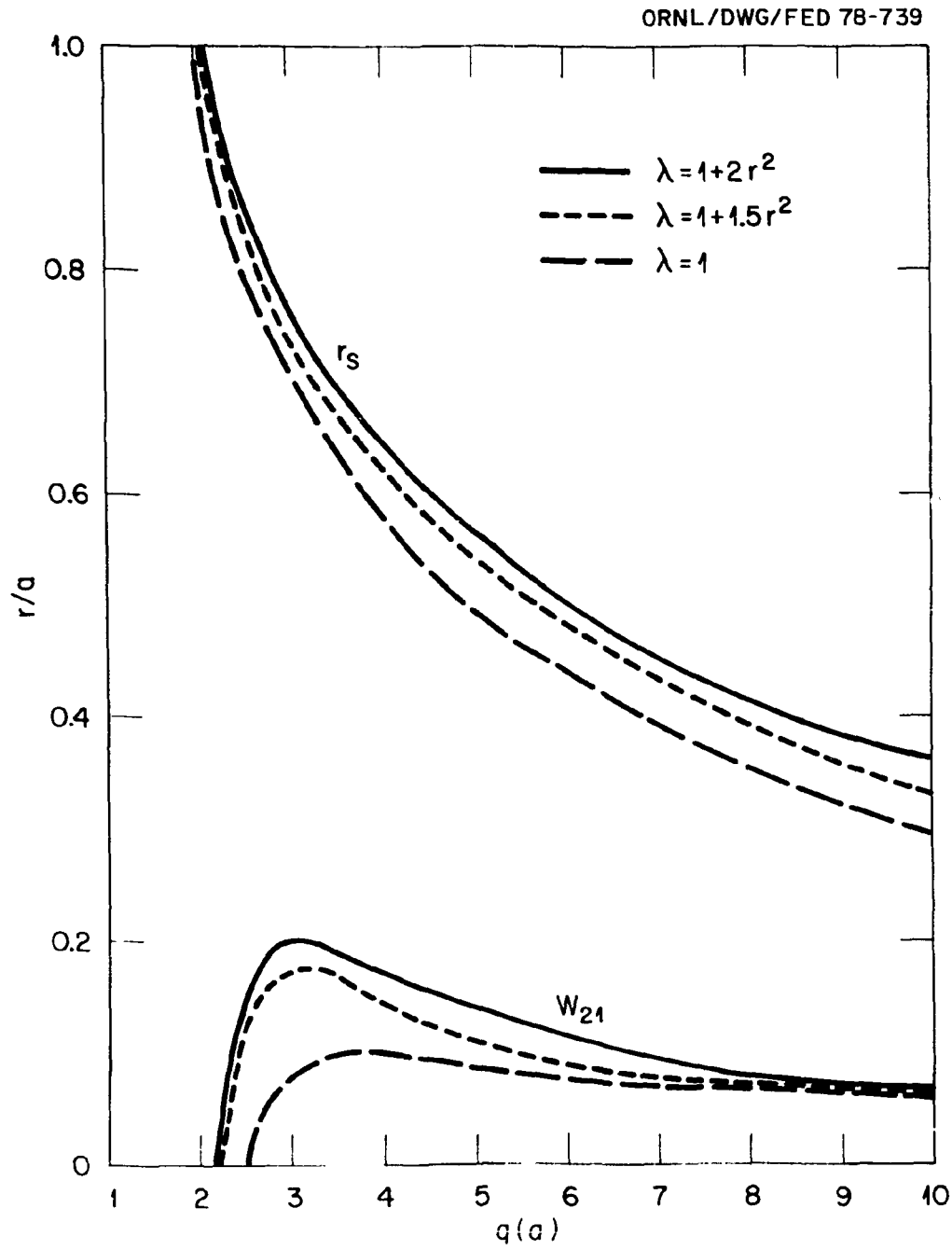
ORNL/DWG/FED 78-739
1.0
0.8
0.6
0.4
0.2
0
r/a
λ=1+2r²
λ=1+1.5r²
λ=1
rs
W21
1
2
3
4
5
6
7
8
9
10
q(a)

Fig. 3(a).

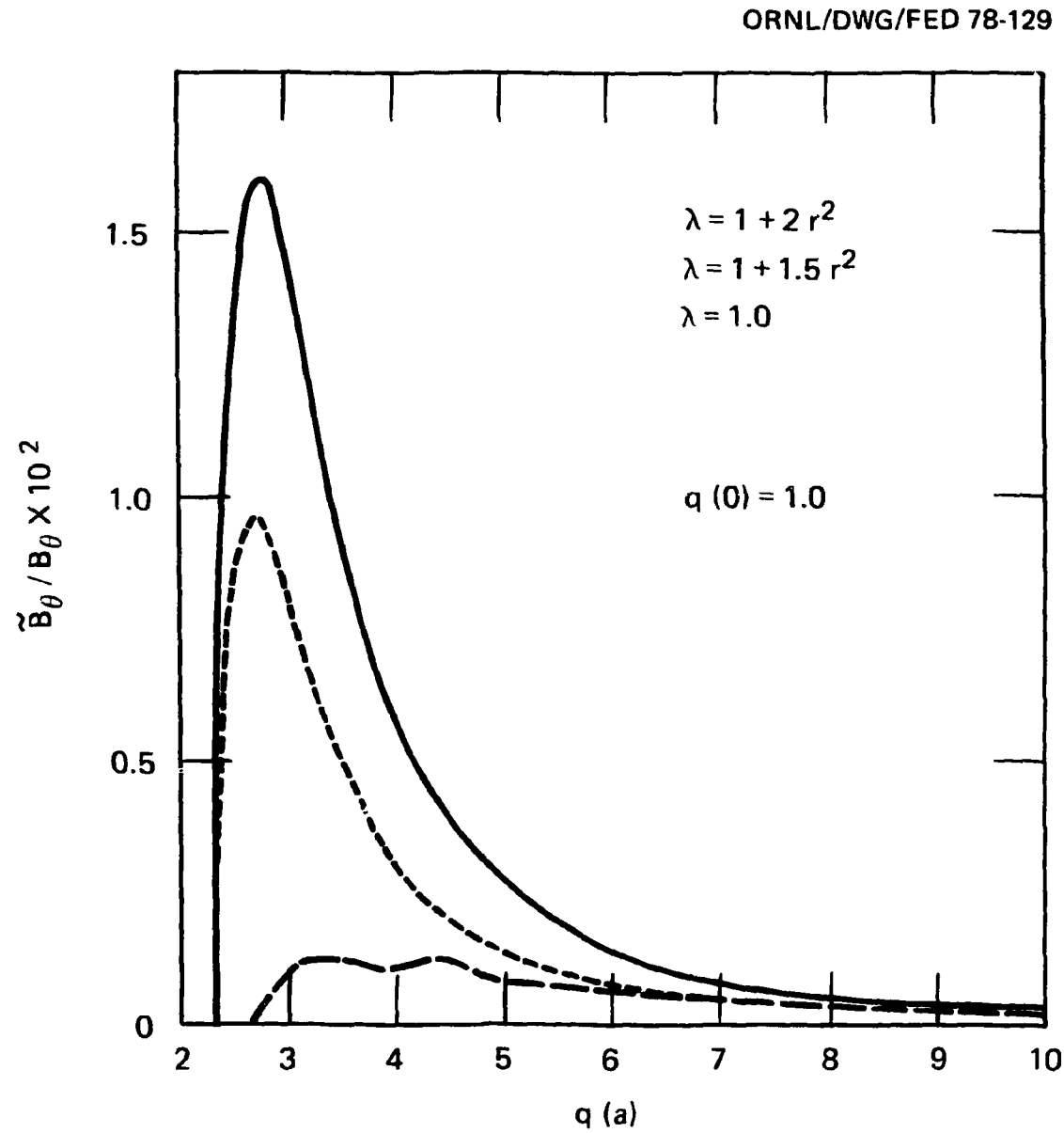
ORNL/DWG/FED 78-129
$\lambda = 1 + 2\,r^2$
$\lambda = 1 + 1.5\,r^2$
$\lambda = 1.0$
q (0) = 1.0
$\tilde{B}_\theta / B_\theta \times 10^2$
1.5
1.0
0.5
0
2
3
4
5
6
7
8
9
10
q (a)

Fig. 3(b).

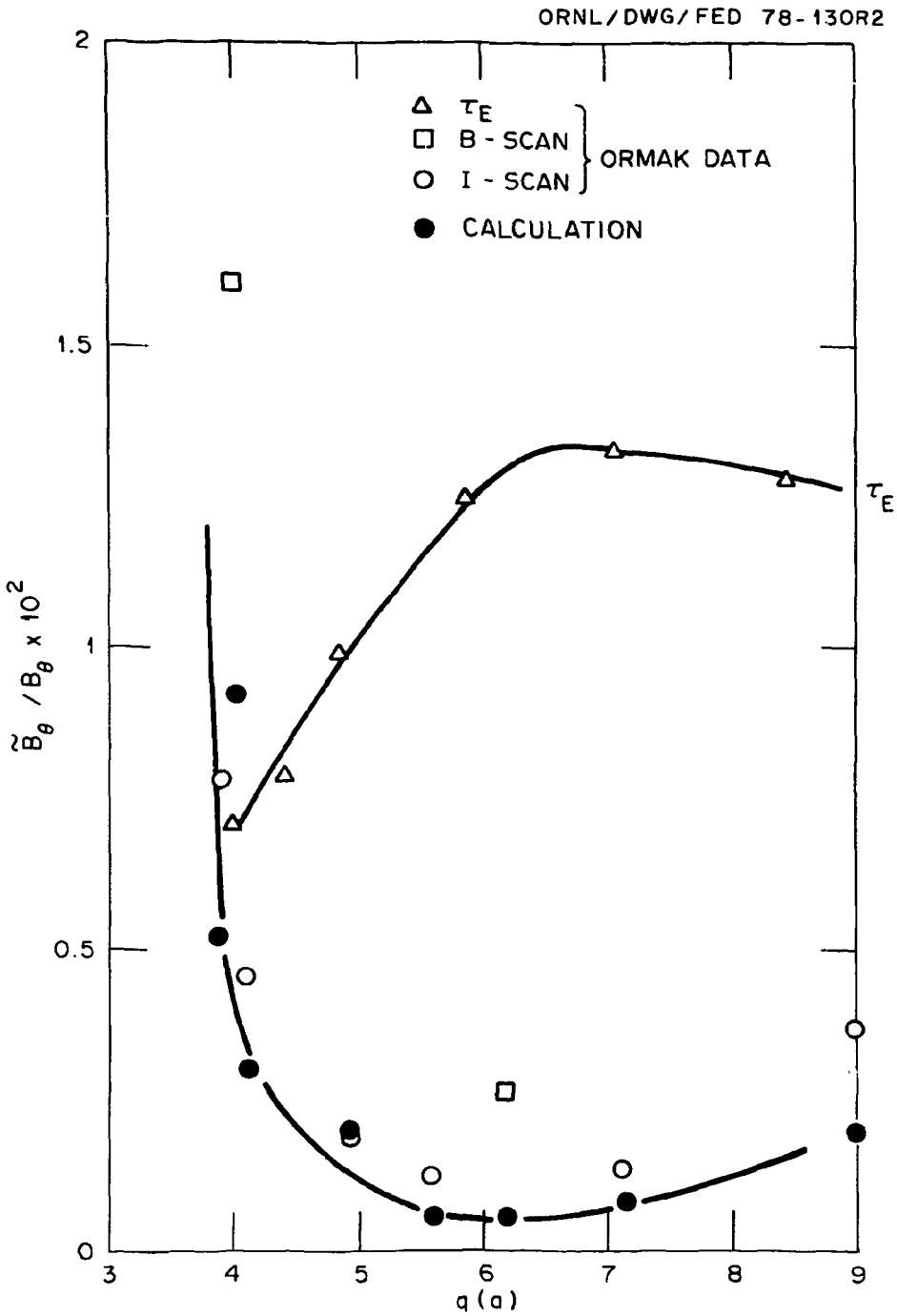
ORNL/DWG/FED 78-130R2
τ_E
B - SCAN
I - SCAN
ORMAK DATA
CALCULATION
$\tilde{B}_\theta / B_\theta \times 10^2$
τ_E
q(a)
0
0.5
1
1.5
2
3
4
5
6
7
8
9

Fig. 4.

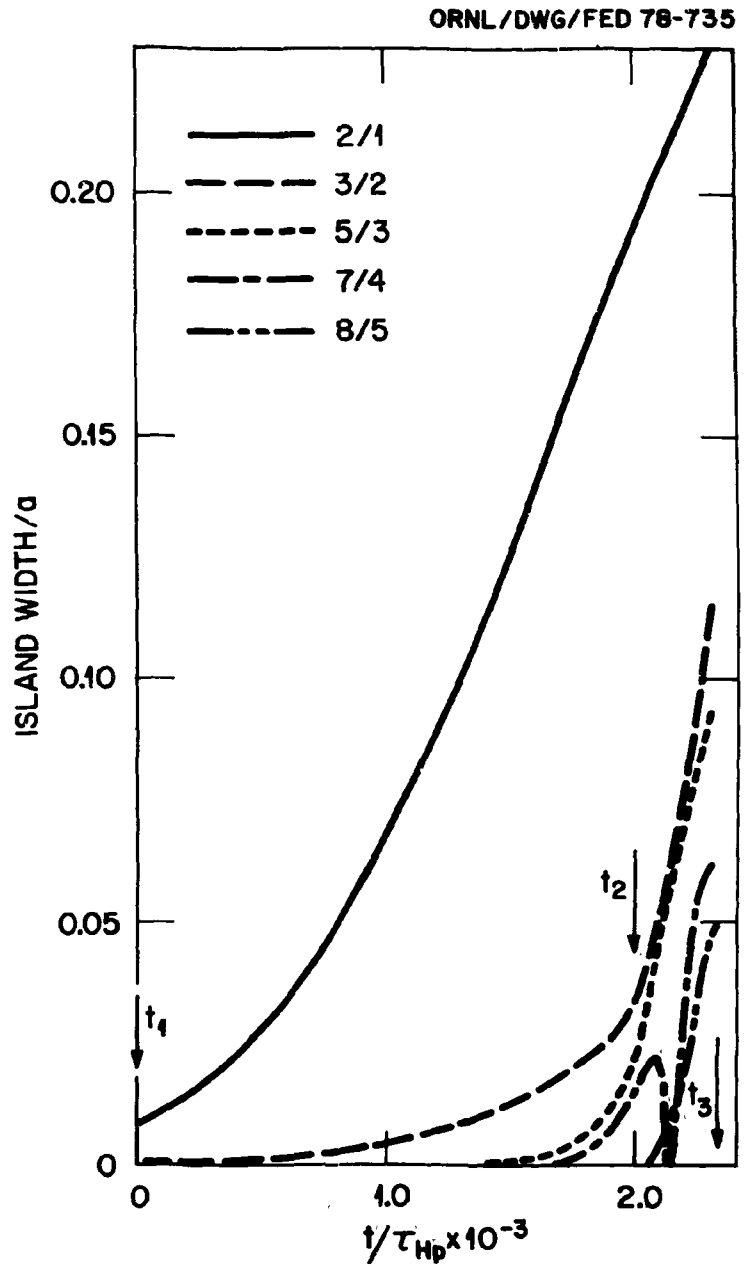
ORNL/DWG/FED 78-735
2/1
3/2
5/3
7/4
8/5
0.20
0.15
0.10
0.05
0
ISLAND WIDTH/a
t1
t2
t3
0
1.0
2.0
t/τHp x 10-3

Fig. 5(a).

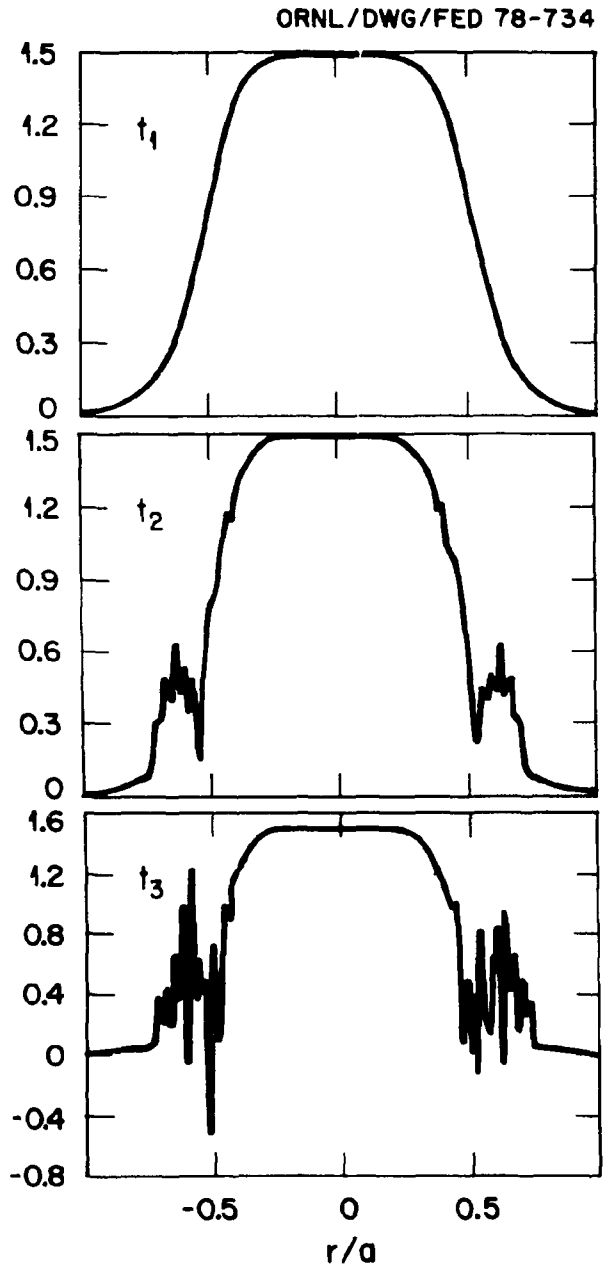
ORNL/DWG/FED 78-734
1.5
1.2
0.9
0.6
0.3
0
t_1
1.5
1.2
0.9
0.6
0.3
0
t_2
1.6
1.2
0.8
0.4
0
-0.4
-0.8
t_3
-0.5
0
0.5
r/a

Fig. 5(b).

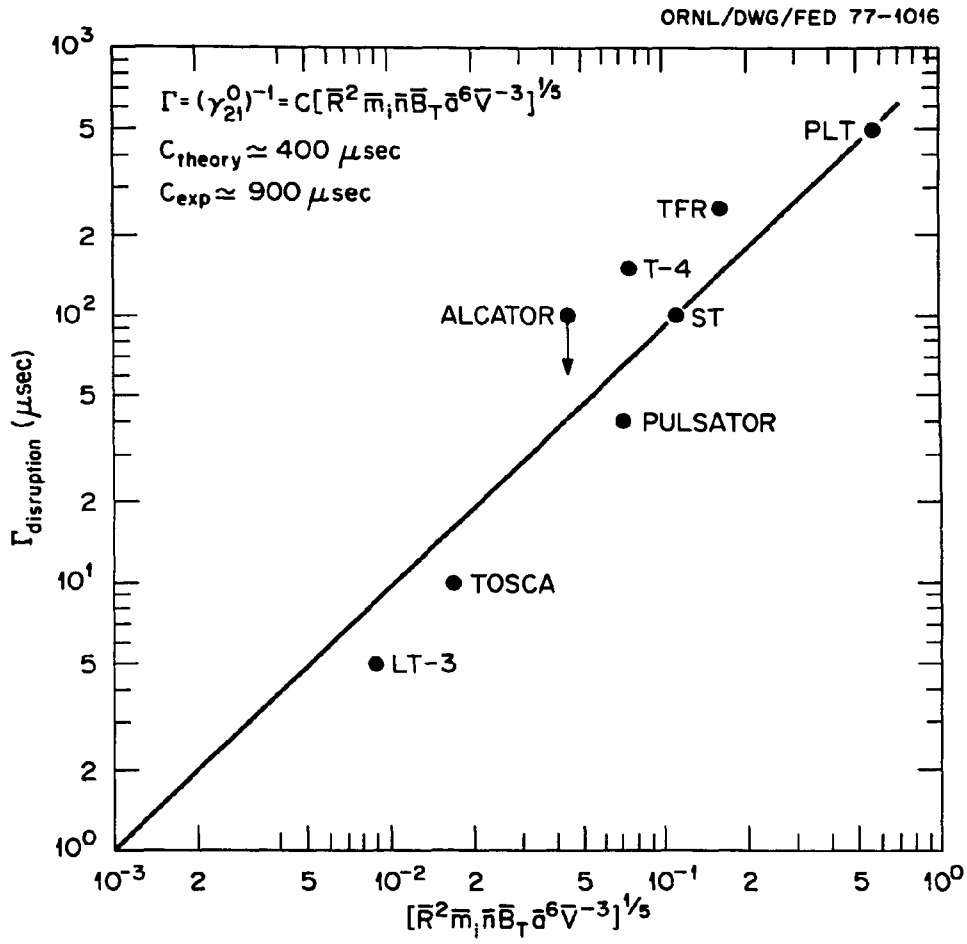
ORNL/DWG/FED 77-1016
$\Gamma = (\gamma_{21}^0)^{-1} = C[\bar{R}^2 \bar{m}_i \bar{n} \bar{B}_T \bar{a}^6 \bar{V}^{-3}]^{1/5}$
$C_{theory} \simeq 400\ \mu sec$
$C_{exp} \simeq 900\ \mu sec$
PLT
TFR
T-4
ALCATOR
ST
PULSATOR
TOSCA
LT-3
$\Gamma_{disruption}$ (μsec)
$[\bar{R}^2 \bar{m}_i \bar{n} \bar{B}_T \bar{a}^6 \bar{V}^{-3}]^{1/5}$

Fig. 6.

ORNL/TM-6564
Dist. Category UC-20 f and g

INTERNAL DISTRIBUTION

1. L. A. Berry
2. J. D. Callen
3. R. A. Dandl
4. R. A. Dory
5. G. G. Kelley
6. H. H. Haselton
7. P. N. Haubenreich
8. M. S. Lubell
9. O. B. Morgan
10. H. Postma
11. M. W. Rosenthal
12. J. Sheffield
13. D. Steiner
14-46. J. D. Callen
47-48. Laboratory Records Department
49. Laboratory Records, ORNL-RC
50. Document Reference Section
51-52. Central Research Library
53. Fusion Energy Division Library
54. Fusion Energy Division Communications Center
55. ORNL Patent Office

EXTERNAL DISTRIBUTION

56. D. J. Anthony, Energy Systems and Technology Division, General Electric Company, 1 River Road, Bldg. 23, Room 290, Schenectady, NY 12345
57. Bibliothek, Max-Planck Institute für Plasmaphysik, 8046 Garching bei München, Federal Republic of Germany
58. Bibliothèque, Service du Confinement des Plasmas, C.E.A., B.P. No. 6, 92, Fontenay-aux Roses (Seine), France
59. Lung Cheung, Department of Electronics, University Science Center, The Chinese University of Hong Kong, Shatin, N.T., Hong Kong
60. J. F. Clarke, Office of Fusion Energy, G-234, Department of Energy, Washington, DC 20545
61. R. W. Conn, Fusion Technology Program, Nuclear Engineering Department, University of Wisconsin, Madison, WI 53706
62. CTR Library, c/o Alan F. Haught, United Technologies Research Laboratory, East Hartford, CT 06108
63. CTR Reading Room, c/o Allan N. Kaufman, Physics Department, University of California, Berkeley, CA 94720
64. J. Narl Davidson, School of Nuclear Engineering, Georgia Institute of Technology, Atlanta, GA 30332
65. Documentation S.I.G.N., Département de la Physique du Plasma et de la Fusion Controlée, Association EURATOM-CEA sur la Fusion, Centre d'Études Nucléaires, B.P. 85, Centre du TRI, 38041 Grenoble, Cedex, France
66. W. R. Ellis, Office of Fusion Energy, G-234, Department of Energy, Washington, DC 20545
67. Harold K. Forsen, Exxon Nuclear Co., Inc., 777 106th Avenue, N.E., C-000777, Bellevue, WA 98009
68. Harold P. Furth, Princeton Plasma Physics Laboratory, Princeton University, Forrestal Campus, P.O. Box 451, Princeton, NJ 08540
69. Roy W. Gould, California Institute of Technology, Mail Stop 116-81, Pasadena, CA 91125

BLANK PAGE

70. Robert L. Hirsch, Exxon Research and Engineering, P.O. Box 101, Florham Park, NJ 07932
71. Raymond A. Huse, Manager, Research and Development, Public Service Gas and Electric Company, 80 Park Place, Newark, NJ 07101
72. T. Hsu, Office of Fusion Energy, G-234, Department of Energy, Washington, DC 20545
73. V. E. Ivanov, Physical-Technical Institute of the Ukranian Academy of Sciences, Sukhumi, U.S.S.R.
74. A. Kadish, Office of Fusion Energy, G-234, Department of Energy, Washington, DC 20545
75. L. M. Kovrizhnikh, Lebedev Institute of Physics, Academy of Sciences of the U.S.S.R., Leninsky Prospect 53, Moscow, U.S.S.R.
76. Guy Laval, Groupe de Physique Théorique, Ecole Polytechnique, 91 Palaiseau, Paris, France
77. Library, Centre de Recherches en Physique des Plasma, 21 Avenue des Bains, 1007, Lausanne, Switzerland
78. Library, Culham Laboratory, United Kingdom Atomic Energy Authority, Abingdon, Oxon, OX14 3DB, United Kingdom
79. Library, FOM-Institut voor Plasma-Fysica, Rijnhuizen, Jutphaas, Netherlands
80. Library, Institute for Plasma Physics, Nagoya University, Nagoya, Japan 464
81. Library, International Centre for Theoretical Physics, Trieste, Italy
82. Library, Laboratorio Gas Ionizzati, Frascati, Italy
83. Dsumber G. Lominadze, Academy of Sciences of the Georgian S.S.R., 8 Dzerzhinski St., 38004, Tbilisi, U.S.S.R.
84. Oscar P. Manley, Office of Fusion Energy, G-234, Department of Energy, Washington, DC 20545
85. D. G. McAlees, Exxon Nuclear Co., Inc., Research and Technology Laser Enrichment Department, 2955 George Washington Way, Richland, WA 99352
86. J. E. McCune, School of Engineering, Department of Aeronautics and Astronautics, Bldg. 37-391, Massachusetts Institute of Technology, Cambridge, MA 02139
87. Claude Mercier, Service du Theorie des Plasmas, Centre d'Études Nucléaires, Fontenay-aux-Roses (Seine), France
88. K. G. Moses, Office of Fusion Energy, G-234, Department of Energy, Washington, DC 20545
89. R. E. Papsco, Grumman Aerospace Corp., 101 College Road, Princeton, NJ 08540
90. D. Pfirsch, Institute for Plasma Physics, 8046 Garching bei München, Federal Republic of Germany
91. Plasma Physics Group, Department of Engineering Physics, Australian National University, P.O. Box 4, Canberra A.C.T. 2600, Australia
92. A. Rogister, Institute for Plasma Physics, KFA, Postfach 1913, D-5170, Jülich 1, Federal Republic of Germany
93. W. Sadowski, Office of Fusion Energy, G-234, Department of Energy, Washington, DC 20545

94. V. D. Shafranov, I. V. Kurchatov Institute of Atomic Energy, 46 Ulitsa Kurchatova, P.O. Box 3402, Moscow, U.S.S.R.
95. Yu. S. Sigov, Institute of Applied Mathematics of the U.S.S.R. Academy of Sciences, Miuskaya, Sq. 4, Moscow A-47, U.S.S.R.
96. W. M. Stacey, Jr., School of Nuclear Engineering, Georgia Institute of Technology, Atlanta, GA 30332
97. J. B. Taylor, Culham Laboratory, United Kingdom Atomic Energy Authority, Abingdon, Oxon, OX14 3DB, United Kingdom
98. Thermonuclear Library, Japan Atomic Energy Research Institute, Tokai, Naka, Ibaraki, Japan
99. Francisco Verdaguer, Director, Division of Fusion, Junta de Energia Nuclear, Madrid 3, Spain
100. Director, Research and Technical Support Division, Department of Energy, Oak Ridge Operations, P.O. Box E, Oak Ridge, TN 37830
101-349. Given distribution as shown in TID-4500, Magnetic Fusion Energy (Distribution Category UC-20 f and g, Experimental Plasma Physics and Theoretical Plasma Physics)